SPECIAL ISSUE

CSIRO PUBLISHING

*Environ. Chem.*
http://dx.doi.org/10.1071/EN16192

Research Paper

# Doped Ti-pillared clays as effective adsorbents – Application to methylene blue and trimethoprim removal

*Beatriz González,*[A] *Raquel Trujillano,*[A] *Miguel A. Vicente,*[A,D] *Vicente Rives,*[A] *Emerson H. de Faria,*[B] *Katia J. Ciuffi,*[B] *Sophia A. Korili*[C] *and Antonio Gil*[C]

[A]Grupo de Investigación Reconocido Química del Estado Sólido, Materiales y Catálisis Heterogénea (GIR-QUESCAT), Departamento de Química Inorgánica, Universidad de Salamanca, 37008 Salamanca, Spain.
[B]Universidade de Franca, Avenida Dr Armando Salles Oliveira, Parque Universitário, 201, 14404-600, Franca/SP, Brazil.
[C]Departamento de Química Aplicada, Universidad Pública de Navarra, Campus de Arrosadía, E-31006-Pamplona, Spain.
[D]Corresponding author. Email: mavicente@usal.es

**Environmental context.** Water is an essential compound for life; however, several factors limit the amount available for human consumption. Every day, thousands of pollutants are discharged into drinking water. Here, new materials that are efficient as adsorbents and photocatalysts for pollutants are reported.

**Abstract.** Montmorillonite was treated with Ti-based solutions doped with various transition metal cations, leading after calcination at 500 °C to new doped Ti-pillared montmorillonite solids. These solids were characterised by elemental chemical analysis, powder X-ray diffraction, Fourier-transform (FT)-IR spectroscopy, thermal analyses, nitrogen adsorption, acidity evaluation and electron microscopy. The performance of these solids in the degradation of methylene blue and the adsorption of trimethoprim was evaluated.

**Additional keywords:** montmorillonite, Ti-PILC, trimethoprim adsorption.

Received 25 November 2016, accepted 18 February 2017, published online 9 March 2017

## Introduction

Water is one of the most abundant compounds in Nature, covering approximately three-quarters of the Earth's surface. Despite its apparent abundance, several factors limit the amount of drinkable water available for human consumption. Human activities can affect water quality in many different ways by addition of chemical and biological pollutants and biodegradable and non-biodegradable substances, causing illness, disability, death and even disappearance of animal and plant species.[1] So, removal of environmental pollutants is essential because of their harmful effects on ecosystems. There are now several methods proposed for the treatment of contaminated wastewater such as solvent extraction, reverse osmosis, advanced oxidation and adsorption.[2–5] Adsorption on porous materials with a high specific surface area has been the predominant method owing to its low initial cost, simplicity of design, versatility, ease of operation, and insensitivity to toxic substances.[6,7] However, adsorption implies the change of the pollutant from the liquid to the solid phase, but not its degradation, which is highly desirable.

Development of new materials and technologies for removal of organic and inorganic emerging contaminants (EC) is a key point for sustainability of the environment and also for human health. A large number of non-regulated ECs has been detected, mainly in the nanogram per litre to microgram per litre range, in surface waters across Europe. Recently, more than 200 different pharmaceuticals were reported in river waters, with concentrations up to a maximum of 6.5 mg $L^{-1}$ for ciprofloxacin.[8] The increasing spread in the environment of antibiotic-resistant bacteria caused by the presence of antibacterial drugs is a crucial health concern.[9]

The use of sunlight as a source of energy for the removal of pollutants in wastewater has aroused great interest. Emerging contaminants (pharmaceuticals, steroids and hormones, personal-care products, antiseptics, surfactants…) have to be removed in wastewater treatment plant effluents.[10] New efficient materials based on titanium-pillared montmorillonite efficient as photocatalysts for and adsorbents of pollutants are reported in the present paper. These solids have been tested for removal of methylene blue and trimethoprim. Methylene blue (MB) is a heterocyclic aromatic chemical compound (a phenothiazine derivative) with the chemical formula $C_{16}H_{18}N_3SCl$. It is a component of a frequently prescribed urinary analgesic, anti-infective and antispasmodic known as Prosed®/DS. Trimethoprim ($C_{14}H_{18}N_4O_3$, TMP) is a bacteriostatic antibiotic derived from trimethoxybenzylpyrimidine and almost exclusively used in the treatment of urinary tract infections. Trimethoprim belongs to a group of chemotherapeutic agents known as dihydrofolate reductase inhibitors.

The concentration of TMP in wastewater has been reported to be in the microgram per litre range. Thus, values of

0.66–0.71 μg $L^{-1}$,[11] 0.6–7.6 μg $L^{-1}$ in Swedish hospital sewage water,[12] 0.12–0.16 μg $L^{-1}$ in East Aurora and Holland wastewater effluents,[13] and 0.013–0.15 μg $L^{-1}$ in US streams[14] have been found. Additionally, a study carried out in Australia showed that TMP was detected 50 m from a site of discharge, even finding bacteria (*Escherichia coli*) resistance to TMP.[15] Adsorption has been used by some authors for removal of TMP. A maximum adsorption capacity of 0.89–1.12 mmol $g^{-1}$ of TMP on a commercial carbon was reported, dependent on the particle size,[16] whereas 0.41–1.19 mmol $g^{-1}$ was adsorbed by pyrolysed and activated lotus stalks[17] and 0.31 mmol $g^{-1}$ by sewage sludge and fish waste-based adsorbents.[18] Using a montmorillonite clay, adsorption of 0.14–0.44 mmol $g^{-1}$ was found.[19]

It is estimated that more than 100 000 commercially available dyes with over $7 \times 10^5$ tonnes of dyestuff are produced annually.[20] Public perception of water quality is greatly influenced by its colour. The presence of even very small amounts of dyes in water – less than 1 mg $L^{-1}$ for some dyes – is highly visible and undesirable.[21,22] The rate of colour removal depends on the concentration of reactants, pH, ionic strength and surfactant concentration; it is also important for the supported catalysts to be very stable and reusable.[23] So, a removal efficiency of 98 % for MB at pH 4 using kaolin and 100 % at pH 5 using zeolite has been reported,[24] and 100 % at natural pH 6.9 and with an adsorbent dose of 600 mg per 50 mL of 10-mg $L^{-1}$ dye concentration for coir pith carbon.[25] Using $TiO_2$–montmorillonite under UV irradiation, 95 % removal has been found.[26]

Montmorillonite (Mt) is a layered clay mineral belonging to the smectite group, able to absorb or exchange molecules or cations between its layers and to adsorb them on the external surface. An important disadvantage of smectites is the difficulty in controlling a permanent interlayer space, as the layers collapse on dehydration at 250 °C, hindering access to the interlayer space and limiting their applicability. The intercalation of large polyoxocations and the subsequent calcination of the solids thus obtained give rise to stable structures with constant interlayer spaces up to high temperatures. This process, called pillaring, allows solids (pillared clays, PILC) with an adequate porosity to be used as catalysts and adsorbents to be obtained.[27,28] The pillars constitute the most active phase in these solids, while the layers mainly act as supports for this ultradispersed phase. $TiO_2$ is the most popular photocatalyst, owing to its high performance, low cost, chemical inertness, photostability and biocompatibility,[29] being largely used in the degradation of pollutants by photocatalysis.[30,31] $TiO_2$ can be incorporated into smectites by pillaring, and in some cases, higher activity has been reported for Ti-pillared clays than for $TiO_2$ powder particles.[32] Incorporation of Ti into clays forming porous clay heterostructures (PCHs) has recently been reported,[33] and the addition of small concentrations of doping cations is expected to enhance the activity of titania pillared materials.

In the present paper, the use of titanium-pillared Mt to adsorb MB or TMP from aqueous solutions is reported. To this end, doping cations were incorporated into titanium-pillared Mt, studying the changes in the structural, textural and surface properties compared with those for the undoped titanium pillared clay, and also the change in photocatalytic properties by changing the band gap of $TiO_2$. In order to reach this target, Ti solutions were doped with a series of different cations, namely $Fe^{3+}$, $Cr^{3+}$, $Cu^{2+}$, $Ag^+$, $Nd^{3+}$ and $In^{3+}$ before the polymerisation step, in order to attain a later incorporation of these metal cations into the final titanium-Mt pillared nanocomposite; how clay functionalisation affected the capacity of Mt to adsorb MB or TMP was also studied. The incorporation of these metal cations and their influence on the properties of the final solids are discussed.

## Materials and methods

### Source material

The clay mineral used in this work was a raw Mt from Cheto, Arizona, USA (The Clay Minerals Repository, reference code SAz-1). The natural clay mineral was purified before its use by dispersion–decantation, separating the ≤2-μm fraction. Its cation exchange capacity was 0.67 mequiv. $g^{-1}$, its basal spacing 13.60 Å and its Brunauer–Emmett–Teller (BET) specific surface area ($S_{BET}$) 49 $m^2$ $g^{-1}$.[34]

### Preparation of the solids

The preparation of the Ti-pillared Mt was carried out adapting the method proposed by Lin et al.[35] A titanium polycation solution, $[(TiO)_8(OH)_{12}]^{4+}$,[36] was prepared by slow addition, under vigorous stirring, of 11 mL of $TiCl_4$ (Sigma-Aldrich, Madrid, Spain) to 22 mL of absolute ethanol (Panreac, Madrid, Spain), until a homogeneous yellowish solution was obtained. This solution was added to a previously prepared solution of 25 mL of glycerine (Panreac) in 25 mL of distilled water. The new mixture stirred for 3 h, and then a portion of 8 mL was added dropwise to a previously prepared Mt aqueous suspension with a Ti/clay ratio of 40 mmol $g^{-1}$, aging the new suspension under magnetic stirring for 18 h. Then, the solid was separated by centrifugation, washed by dialysis for 2 days, dried overnight at 70 °C and calcined at 500 °C for 2 h at a heating rate of 1 °C $min^{-1}$. For the doped solids, an appropriate amount of the dopant cations was added to the $TiCl_4$ solution, using two $Ti^{4+}$/doping cation atomic ratios, namely, 90 : 10 and 95 : 5. $CrCl_3 \cdot 6H_2O$, ferric citrate, $Cu(NO_3)_2 \cdot 3H_2O$, $AgNO_3$, $NdCl_3 \cdot 6H_2O$ and $In(NO_3)_3 \cdot xH_2O$ were used as precursor salts (salts of silver and copper were supplied by Panreac, and all the other reagents by Sigma-Aldrich, having the higher purity degree available and were used without any treatment). The preparation procedure was the same as described for the Ti solid. The solid pillared with only Ti is designated MtTi, and the doped pillared solids are designated by adding the symbol of the doping cation and its atomic percentage content; for instance, MtTiCr10 corresponds to the solid obtained by treatment of Mt with a solution containing 10 mol-% $Cr^{3+}$ and 90 mol-% $Ti^{4+}$.

### Characterisation techniques

Elemental chemical analyses were carried out by inductively coupled plasma–atomic emission spectrometry (ICP-AES) at Activation Laboratories Ltd (Ancaster, ON). The powder X-ray diffraction patterns were obtained over non-oriented powder samples, in the $2\theta$ range from 2 to 65°, at a scanning speed of 2° $min^{-1}$. The instrument used was a Siemens D-500 diffractometer, operating at 40 kV and 30 mA, with filtered Cu K$\alpha$ radiation ($\lambda$ = 1.5418 Å). Fourier-transform (FT)-IR spectra were recorded in the 450–4000 $cm^{-1}$ range on a PerkinElmer Spectrum-One spectrometer. Approximately 1 mg of sample and 300 mg of KBr were used in the preparation of the pellets. Thermal analyses were conducted on a SDT Q600 TA instrument. All measurements were carried out under a flow of 20 mL $min^{-1}$ of oxygen (99.999 %, Air Liquide, Madrid, Spain) and a heating rate of 10 °C $min^{-1}$ from room temperature up to

900 °C. The textural properties were determined from the nitrogen (Air Liquide, 99.999 %) adsorption–desorption isotherms at −196 °C using a Micrometrics Gemini VII 2390 surface area and porosity apparatus. The samples (0.1 g) were degassed at 110 °C for 2 h. The specific surface area was calculated by the BET method, the external surface area and micropore volume by the *t*-method, and the total pore volume from the amount of nitrogen adsorbed at a relative pressure of 0.95.[37–39]

The acidity was determined by adsorption of pyridine and heating at increasing temperatures, following the process by FT-IR spectroscopy. Solids (20 mg) were exposed to pyridine vapour in a desiccator for 1 h. Then, FT-IR wafers were prepared using a sample/KBr mass ratio of 10 : 600. The spectra were recorded after outgassing the wafers under vacuum at room temperature, and after heating them for 1 h at 100, 200, 300, 400 and 500 °C in an open system, in each case followed by cooling under vacuum. The spectra were recorded using the spectrometer mentioned above. The number of Brönsted and Lewis acid sites was evaluated using Eqn 1, proposed by Barzetti et al. and successfully applied to clay materials by Del Rey Pérez-Caballero and Poncelet:[40,41]

$$q_{B,L} = \frac{A_{B,L}\pi R^2}{\omega \varepsilon_{B,L}} \quad (1)$$

where $q_{B,L}$ is the concentration (μmol $g^{-1}$) of Brönsted or Lewis acid sites, $R$ is the radius of the wafer (cm), $\omega$ is the wafer mass (g), $A_{B,L}$ is the integrated area of the bands at 1545 $cm^{-1}$ (for Brönsted sites) and 1450 $cm^{-1}$ (for Lewis sites), and $\varepsilon_{B,L}$ is the extinction coefficient, for which the values reported by Emeis were used, 1.67 ± 0.12 and 2.22 ± 0.21 cm $\mu mol^{-1}$ for Brønsted and Lewis sites respectively.[42]

The study of the samples by scanning electron microscopy (SEM) of the solids was performed at the Pulsed Laser Centre (CLPU, Salamanca, Spain) using a Carl Zeiss SEM EVO HD25 microscope. The samples were coated with a thin gold layer using a Bio-Rad ES100 SEN coating system.

### *Removal of methylene blue*

Removal studies were carried out by determining the amount of MB that was eliminated after 24 h by means of experiments using 5.0 mL of a 500-mg $L^{-1}$ MB (Sigma-Aldrich) solution and 50 mg of the adsorbent under constant stirring (initial pH of the solutions was 5.7, not controlled during the experiments). The experiments were carried out under exposure to UV radiation ($\lambda$ = 365 nm, power = 30 W) or without light, using the same chamber but maintained completely in darkness. Then, the clay was separated from the supernatant liquid by centrifugation at 1650 *g* for 10 min at room temperature, and MB concentration was determined by measuring the absorbance of the solutions at 665 nm, the wavelength of maximum absorbance for MB. After finishing the process, the solids were filtered, washed with distilled water 5–6 times, dried, and used in a second adsorption cycle, both with or without light and under the same conditions. All experiments were carried out in duplicate, and the values given are the average of both measurements.

### *Adsorption of trimethoprim*

The adsorption kinetics experiments were carried out in glass vials by shaking a known amount of the adsorbent, typically 50 mg, with 5.0 mL of an ethanol/water (1 : 1) trimethoprim (≥98 %, Sigma-Aldrich) solution (100 mg $L^{-1}$). The suspensions were stirred at room temperature in the dark for a predetermined period of time (between 1 and 90 min for intercalated samples and between 1 and 270 min for the natural clay). Then, the clay was separated from the supernatant liquid by centrifugation at 1650 *g* for 10 min at room temperature. UV-visible spectroscopy (Thermo Electron Helios Gamma spectrophotometer) was used to determine the concentration of trimethoprim in the solutions from their absorbance at 289 nm, the wavelength corresponding to the maximum absorbance of TMP. Calibration had been previously carried out with TMP solutions at concentrations ranging between 1 and 50 mg $L^{-1}$, the range used in the adsorption experiments and in which absorbance shows a linear response with concentration, following the Beer–Lambert law. After determining the TMP concentration in the supernatant liquid, the amount adsorbed onto the solid was calculated according to Eqn 2:

$$q_t = \frac{V(C_i - C_t)}{m} \quad (2)$$

where $q_t$ (mg $g^{-1}$) is the amount of TMP adsorbed at time $t$ (min), $C_i$ (mg $mL^{-1}$) the initial concentration in the solution, $C_t$ (mg $mL^{-1}$) the concentration at time $t$, $V$ (mL) the volume of the solution, and $m$ (g) the amount of adsorbent.

The adsorption equilibrium experiments were carried out in glass vials at room temperature by shaking 50 mg of the adsorbent with 5.0 mL of TMP aqueous solution at the selected concentration, between 1 and 400 mg $L^{-1}$ (although the initial concentration was up to 400 mg $L^{-1}$, the equilibrium concentration was always within the calibration range). The vials containing the TMP solution and the adsorbent were shaken for 5 or 10 min for MtTiFe and MtTiCr photocatalysts or 150 min for the natural clay. The amount of adsorbed dye was calculated according to Eqn 3:

$$q_e = \frac{V(C_i - C_e)}{m} \quad (3)$$

where $q_e$ is the amount of trimethoprim adsorbed (mg $g^{-1}$) and $C_e$ (mg $mL^{-1}$) is the equilibrium liquid-phase concentration of TMP.

### *Theoretical approach*

To study the adsorption at equilibrium onto the pillared montmorillonites, the Langmuir, Freundlich and Toth isotherm models were tested.

The Langmuir isotherm describes the adsorption processes as a result of the formation of monolayers on homogeneous surfaces, which occurs on specific adsorption sites of the adsorbent.[43] The isotherm can be mathematically expressed as Eqn 4:

$$q_e = \frac{q_L b C_e}{1 + b C_e} \quad (4)$$

where $q_L$ (mg $g^{-1}$) is a constant related to the monolayer adsorption capacity and $b$ (mL $mg^{-1}$) is the Langmuir constant.

The Freundlich equation is an empirical equation used to describe adsorption on heterogeneous systems.[44] It can be written as:

$$q_e = k_F C_e^{1/n} \quad (5)$$

where $k_F$ and $n$ are empirical constants that represent the extent of adsorption and its efficacy respectively.

The Toth isotherm is used to evaluate equilibrium data for inhomogeneous adsorbents. In this equation, $q_L$ has the same meaning as in the Langmuir isotherm, and $n$ is a parameter that measures the heterogeneity of the system ($0 < n < 1$).[45] When $n = 1$, the Toth isotherm becomes identical to the Langmuir isotherm. Parameters $b$ and $n$ allow independent adjustment of the initial slope and curvature of the isotherm.[46,47] It is usually written as:

$$q_e = \frac{q_T b C}{[1 + (bC)^n]^{1/n}} \quad (6)$$

where $q_T$ (mg/g) is a Toth constant, representing the monolayer adsorption capacity.

## Results and discussion

### *Characterisation of the solids*

Solids composed of Mt pillared with Ti polycations and doped with $Cr^{3+}$, $Fe^{3+}$ and $Cu^{2+}$ have been reported and characterised elsewhere,[34] so only the characterisation data for the $In^{3+}$, $Ag^{+}$ and $Nd^{3+}$-doped solids are reported here.

The elemental chemical compositions of all the doped Ti-PILC samples are given in Table 1. The amount of Ti fixed was in all cases close to 14 % (expressed as $TiO_2$), similar to the values found in the solids doped with $Cr^{3+}$, $Fe^{3+}$ and $Cu^{2+}$,[34] although the amount of the doping elements was clearly lower when using $In^{3+}$, $Ag^{+}$ and $Nd^{3+}$. The polycations are incorporated into the clay structure by cationic exchange of $Ca^{2+}$, its main exchangeable cation, and to a lesser extent of $Na^{+}$ and $K^{+}$ existing in very low amounts in the original Mt.[34] Water is the only volatile species expected in the solids, and its content ranged between 23 and 30 %, so for easy understanding of the changes in the composition of the solids on incorporation of the Ti polycations, a double normalisation was carried out.

First, the composition was given as for water-free solids, that is, the sum of the metal oxides content was normalised to add up to 100 %. Then, the compositions were referred to the content of $SiO_2$ in the original Mt, as the tetrahedral sheet of the clay is probably not affected by the intercalation and pillaring treatment, the amount of $SiO_2$ thus remaining constant, and it can be used as a sort of 'internal standard'. The compositions thus normalised are given in Table 2.

The amount of $TiO_2$ fixed, once the amount existing in the raw Mt was subtracted, was very similar in all the solids, between 21.63 and 26.01 %. The amounts of $Al_2O_3$ and $Fe_2O_3$ remained essentially constant, and that of MgO slightly decreased, thus suggesting that octahedral $Al^{3+}$ and $Fe^{3+}$ were not dissolved, whereas $Mg^{2+}$ was scarcely dissolved. $Ca^{2+}$ was almost completely removed and $Na^{+}$ was partially removed, whereas the $K^{+}$ content remained constant, suggesting that it was in the clay as feldspar, but not as exchangeable cations in Mt. Thus, although the polymerisation of Ti species required

**Table 1. Chemical composition of the solids, expressed as content of their metallic oxides (mass percentage)**
$MO_x$: $Ag_2O$, $Nd_2O_3$ or $In_2O_3$. LOI, loss on ignition, sum of volatile compounds

| | $SiO_2$ | $Al_2O_3$ | $Fe_2O_3$ | MnO | MgO | CaO | $Na_2O$ | $K_2O$ | $TiO_2$ | $MO_x$ | LOI |
|---|---|---|---|---|---|---|---|---|---|---|---|
| Mt | 55.80 | 15.92 | 1.41 | 0.043 | 5.58 | 1.69 | 0.06 | 0.06 | 0.21 | – | 19.22 |
| MtTi | 43.72 | 12.7 | 1.13 | 0.004 | 4.25 | 0.03 | 0.03 | 0.04 | 15.10 | – | 23.00 |
| MtTiAg5 | 43.31 | 11.86 | 1.09 | 0.004 | 3.95 | 0.03 | 0.02 | 0.04 | 14.18 | 0.000064 | 25.52 |
| MtTiAg10 | 41.65 | 11.88 | 1.08 | 0.005 | 3.96 | 0.03 | 0.02 | 0.04 | 13.40 | 0.053 | 27.89 |
| MtTiNd5 | 44.22 | 12.43 | 1.13 | 0.010 | 4.11 | 0.03 | 0.02 | 0.04 | 14.01 | 0.016 | 23.98 |
| MtTiNd10 | 40.47 | 11.61 | 1.07 | 0.015 | 3.91 | 0.03 | 0.02 | 0.03 | 13.10 | 0.031 | 29.71 |
| MtTiIn5 | 44.97 | 12.47 | 1.15 | 0.003 | 4.17 | 0.03 | 0.02 | 0.04 | 14.26 | 0.057 | 22.84 |
| MtTiIn10 | 39.89 | 11.35 | 1.06 | 0.004 | 3.78 | 0.04 | 0.01 | 0.03 | 13.71 | 0.102 | 30.03 |

**Table 2. Chemical composition of the water-free solids, normalised to the $SiO_2$ content in the raw montmorillonite (mass percentage)**

| | $SiO_2$ | $Al_2O_3$ | $Fe_2O_3$ | MnO | MgO | CaO | $Na_2O$ | $K_2O$ | $TiO_2$ | $MO_x$[A] |
|---|---|---|---|---|---|---|---|---|---|---|
| Mt | 69.08 | 19.71 | 1.75 | 0.05 | 6.91 | 2.09 | 0.07 | 0.07 | 0.26 | – |
| MtTi | 69.08 | 20.07 | 1.79 | 0.01 | 6.72 | 0.05 | 0.05 | 0.06 | 23.86 | – |
| MtTiAg5 | 69.08 | 18.91 | 1.73 | 0.01 | 6.30 | 0.05 | 0.04 | 0.06 | 22.62 | 0.0001 |
| MtTiAg10 | 69.08 | 19.70 | 1.79 | 0.01 | 6.57 | 0.05 | 0.04 | 0.07 | 22.22 | 0.08 |
| MtTiNd5 | 69.08 | 19.42 | 1.77 | 0.02 | 6.43 | 0.05 | 0.04 | 0.06 | 21.89 | 0.02 |
| MtTiNd10 | 69.08 | 19.82 | 1.82 | 0.03 | 6.67 | 0.05 | 0.04 | 0.05 | 22.36 | 0.05 |
| MtTiIn5 | 69.08 | 19.15 | 1.77 | 0.01 | 6.40 | 0.05 | 0.04 | 0.06 | 21.90 | 0.08 |
| MtTiIn10 | 69.08 | 19.65 | 1.83 | 0.01 | 6.54 | 0.07 | 0.01 | 0.05 | 23.74 | 0.18 |
| MTiFe5[B] | 69.08 | 19.93 | 1.84 | 0.01 | 6.68 | 0.05 | 0.03 | 0.06 | 24.31 | 0.09 |
| MTiFe10[B] | 69.08 | 20.31 | 1.97 | 0.01 | 6.71 | 0.12 | 0.04 | 0.06 | 26.22 | 0.22 |
| MTiCu5[B] | 69.08 | 19.72 | 1.78 | 0.01 | 6.70 | 0.05 | 0.03 | 0.08 | 24.51 | 0.03 |
| MTiCu10[B] | 69.08 | 19.87 | 1.79 | 0.01 | 6.69 | 0.12 | 0.04 | 0.06 | 26.27 | 0.51 |
| MTiCr5[B] | 69.08 | 20.18 | 1.82 | 0.03 | 6.74 | 0.16 | 0.04 | 0.07 | 25.64 | 0.20 |
| MTiCr10[B] | 69.08 | 20.03 | 1.78 | 0.04 | 6.72 | 0.12 | 0.04 | 0.06 | 24.91 | 0.30 |

[A]$MO_x$: $Ag_2O$, $Nd_2O_3$, $In_2O_3$, $Fe_2O_3$, CuO or $Cr_2O_3$.
[B]From ref. 34.

strong acid conditions, the incorporation of the polycations did not alter the composition of the Mt layers.

The presence of doping metal cations in the Ti solutions led in all cases to lower $TiO_2$ loadings than in the non-doped MtTi solid. In any case, the amount of doping elements fixed in the solids was low. Moreover, in all cases, the amount fixed in the solids was larger when a larger concentration of the doping metal cation was used in the initial solution, and the M/Ti ratio was always lower than the ratio existing in the initial solution. The amounts fixed for $In^{3+}$, $Ag^{+}$ and $Nd^{3+}$ were also lower than those reported for $Cr^{3+}$, $Fe^{3+}$ and $Cu^{2+}$ solids,[34] which may be related to the behaviour of the different cations under the polymerisation conditions used, necessarily very acidic to obtain polymerisation of $Ti^{4+}$. However, the amount of doping elements fixed should still be enough to modify the behaviour of the final solids. Looking at the overall compositions of the final solids, they resembled nanocomposites formed by approximately three parts (by mass) of Mt and one of (doped) $TiO_2$ pillars.

Intercalation with Ti polycations always led to swelling of the interlayer region. The natural Mt had a well-defined basal spacing of 13.60 Å, which collapsed to 9.57 Å after calcination at 500 °C (Fig. 1).[34] The 001 reflection showed a low intensity for all the intercalated solids, indicating that intercalation had a deleterious effect on the ordering of the layers. The basal spacing of the doped solids was always lower than for the solid containing pure $Ti^{4+}$ (17.23–18.60 Å *v.* 19.63 Å, Table 3), suggesting that a lower degree of polymerisation was reached. After calcination at 500 °C, the ordering of the layers continued to be low, but it was slightly better than in the non-doped solid (Fig. 2). Surprisingly, the basal spacing slightly increased on calcination, which is unusual, because calcination implies the dehydration–dehydroxylation of the polycations to form the final pillars, usually decreasing the basal spacing of the solids. In the current case, this finding suggests strong modifications in the polycations during the heating process, probably implying changes in the degree of polymerisation during the first steps of heating. Because the doping cations do not polymerise themselves, they may be incorporated into the Ti polycationic species, because their ionic radii are only slightly greater than that of $Ti^{4+}$, or they may form segregated species; it should be noted that the amount of doping species incorporated is low. The doping cations may strongly alter the polymerisation mechanism of $Ti^{4+}$ in the intercalating solutions and the polycationic species incorporated into the solids may continue their polymerisation during the drying and heating steps, leading finally to higher basal spacings. The basal spacings were very similar when 5 or 10 % concentration of the doping element were compared, except for the case of $In^{3+}$, for which an increase in the concentration of the doping element caused a strong increase in the basal spacing of the pillared solid.

However, the effects due to the in-layer reflections, independent of *c*-stacking, were recorded at the same positions for all the materials, indicating that the layers were not modified, in spite of the strong acidic character of the intercalating solutions. No diffraction effects were observed attributable to crystalline $TiO_2$ phases, or to the doping elements or mixed Ti-doping element phases.

The FT-IR spectra (Fig. 3) were similar for all solids. The O–H stretching band was recorded close to 3443 $cm^{-1}$ and the H–O–H bending vibrational mode at ~1635 $cm^{-1}$. Bands corresponding to the Si–O–Si and Si–O–Al vibrations were recorded at 1042 and 474 $cm^{-1}$, while no M–O (M = Ti, Ag, Nd or In) bands were recorded in the spectra of the pillared clays. The O–H stretching mode at 3600 $cm^{-1}$ increased in intensity

**Table 3. Basal spacing (Å) for intercalated and calcined samples**

| Sample | Intercalated | 500 °C |
|---|---|---|
| Mt | 13.60 | 9.57 |
| MtTi | 19.63 | 18.60 |
| MtTiAg5 | 18.30 | 18.67 |
| MtTiAg10 | 17.27 | 17.94 |
| MtTiNd5 | 17.94 | 19.03 |
| MtTiNd10 | 17.89 | 19.38 |
| MtTiIn5 | 17.23 | 17.23 |
| MtTiIn10 | 18.60 | 20.46 |
| MTiFe5[A] | 19.64 | – |
| MTiFe10[A] | 21.19 | 16.99 |
| MTiCu5[A] | 18.92 | – |
| MTiCu10[A] | 21.14 | 16.49 |
| MTiCr5[A] | 22.03 | – |
| MTiCr10[A] | 22.88 | 16.03 |

[A]From ref. 34.

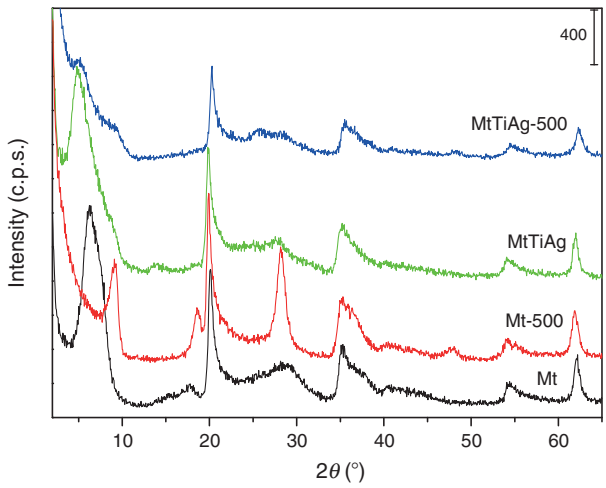


**Fig. 1.** Powder X-ray diffractograms of the natural clay and of the solids intercalated with silver.

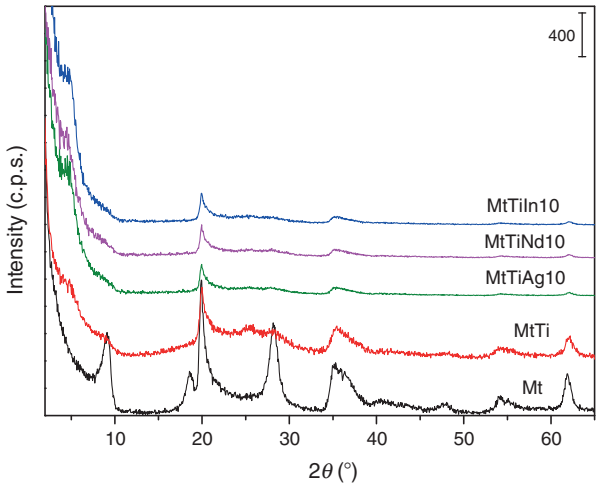


**Fig. 2.** Powder X-ray diffractograms of the pillared solids calcined at 500 °C.

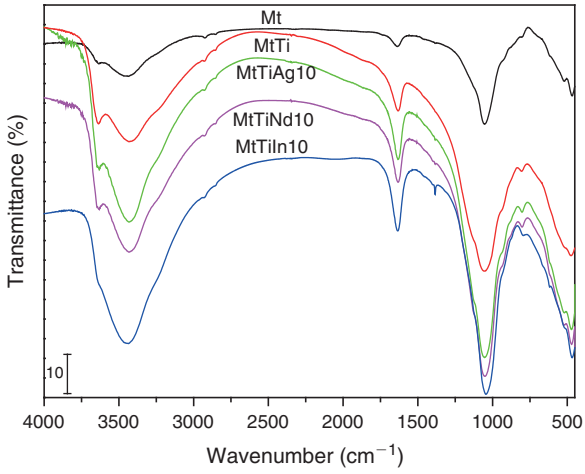


**Fig. 3.** Fourier-transform (FT)-IR spectra of the pillared solids calcined at 500 °C.

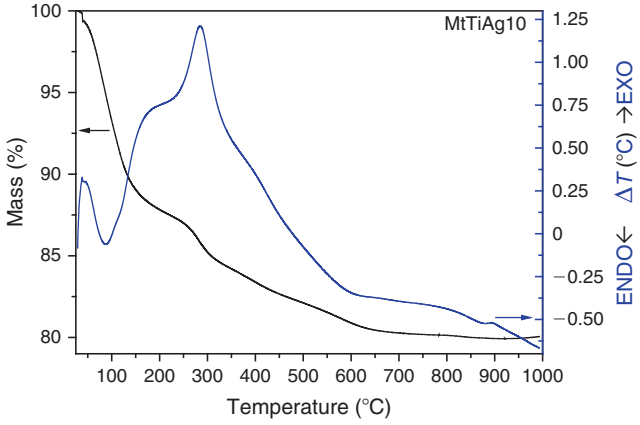


**Fig. 4.** Thermal curves (Thermogravimetry and Differential Thermal Analysis) of MtTiAg10 solid.

and shifted to higher wavenumbers after intercalation, mainly for the $Ag^{+}$ and $Nd^{3+}$-doped solids, showing the interaction of these groups with the polycations. The band characteristic of the tetrahedral layer at 1042 $cm^{-1}$ shifted slightly towards larger wavenumbers too, which is compatible with the removal of octahedral cations under the acidic conditions used for intercalation, because this shift is very typical for acid activation of clay minerals.[48] In the present case, although alteration of the layers was not observable by X-ray diffraction, the removal of a small proportion of the $Mg^{2+}$ was evidenced by the elemental chemical analysis results, as discussed above, and is now confirmed by FT-IR spectroscopy.

The thermogravimetric curves (that for MtTiAg10 is included in Fig. 4 as an example; for comparison, the curves for the MtTi sample are given in Fig. S1) showed mass losses of ~12 % up to ~250 °C associated with an endothermic effect centred close to 80 °C in the differential thermal analysis (DTA) curve, which can be attributed to the removal of water located in the interlayer region, bonded to the polycations or adsorbed on the external surface of the sheets. In the central temperature band, a 7 % mass loss effect was observed associated with several effects in the DTA curve. The most important one caused a clear mass loss and was associated with an exothermic effect

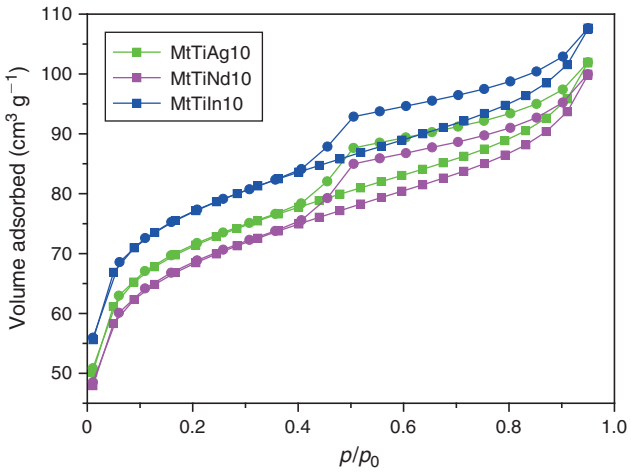


**Fig. 5.** Nitrogen adsorption–desorption isotherms of the pillared solids calcined at 500 °C.

**Table 4. Brunauer–Emmet–Teller specific surface area ($S_{BET}$), external surface area ($S_{ext}$) and micropore volume ($V_m$) of natural montmorillonite and of the pillared solids calcined at 500 °C**

| | $S_{BET}$ ($m^2$ $g^{-1}$) | $S_{ext}$ ($m^2$ $g^{-1}$) | $V_m$ (mL $g^{-1}$) |
|---|---|---|---|
| Mt500 | 80 | 64 | 0.009 |
| MtTi500 | 164 | 80 | 0.047 |
| MtTiAg10–500 | 219 | 104 | 0.064 |
| MtTiNd10–500 | 211 | 104 | 0.059 |
| MtTiIn10–500 | 235 | 105 | 0.072 |
| MTiFe10–500[A] | 300 | 114 | 0.103 |
| MTiCu10–500[A] | 329 | 135 | 0.108 |
| MTiCr10–500[A] | 272 | 124 | 0.082 |

[A]From ref. 34.

centred at 280 °C with a shoulder at 400 °C, which can be attributed to the combustion of organic moieties from the polycations. The Ti polycation usually proposed during polymerisation of $TiCl_4$ with HCl is $[(TiO)_8(OH)_{12}]^{4+}$,[36] whereas for polymerisation of other Ti precursors, mainly alkoxides, the incorporation of organic moieties into the polycations has been claimed,[49,50] although no new complete formulae have been proposed for the polycations. Thus, under the conditions used in the current work, with ethanol and glycerine in the reaction medium, organic species might be coordinated to titanium cations, being a part of the polycations. The removal of structural hydroxyls and a phase change from Mt to mullite was observed as a very weak effect close to 890 °C. No possible effects attributable to the doping elements were observed, as expected from the low amount of these elements fixed in the solids.

The $N_2$ adsorption–desorption isotherms of the solids (Fig. 5) corresponded to type II (IUPAC classification), with a type H4 hysteresis loop at high relative pressure ($p/p_0$) values, typical for solids with narrow slit pores.[51] The loop closed at a relative pressure lower than 0.4, the isotherm being reversible below this relative pressure. The BET specific surface area (Table 4) reached values between 211 and 235 $m^2$ $g^{-1}$ for the solids treated with 10 % of the doping cations after calcination at 500 °C, being significantly higher that the $S_{BET}$ of the undoped Ti counterpart, 164 $m^2$ $g^{-1}$, after calcination at the same

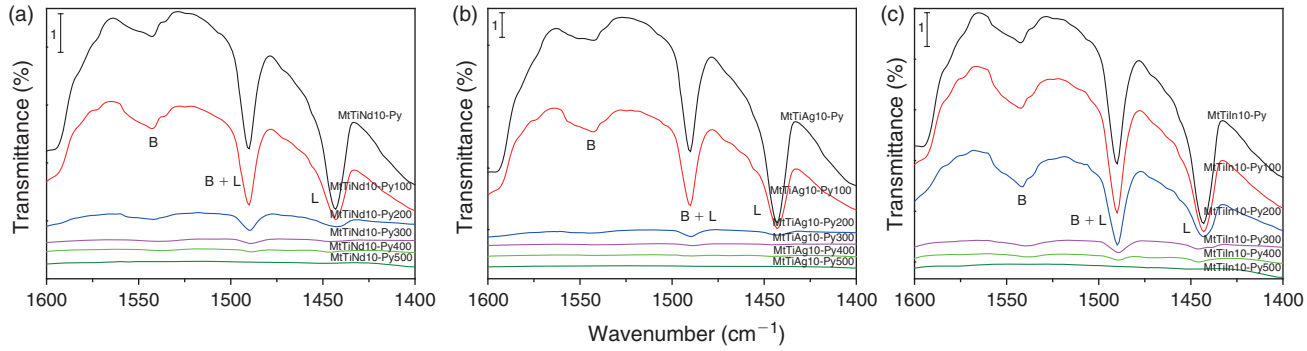


**Fig. 6.** Fourier-transform (FT)-IR spectra of the pillared solids after adsorption of pyridine (py) and heating at increasing temperatures. The solids examined were (a) MtTiNd10, (b) MtTiIn10 and (c) MtTiAg10. For each sample, suffix "-Py" refers to the solid after adsorption of py and the subsequent number indicates the temperature at which py was desorbed. B denotes Brönsted acid sites and L denotes Lewis acid sites.

temperature. This effect should be related to the higher basal spacing of the doped solids, tentatively related to the different polymerisation of $Ti^{4+}$ precursors in the presence of the dopants. The *t*-plots (not shown) had two regions, suggesting a broad distribution of the size of the micropores. Extrapolation of the first part of the curve indicated that the micropore equivalent surface area was in all the solids close to one-half (44–49 %) of the total specific surface area. Accordingly, the pore volume was 0.06–0.07 $cm^3\ g^{-1}$ for the doped solids. All these magnitudes were clearly larger in the doped pillared solids than in the solid pillared with undoped titanium and, of course, much larger than the value for natural Mt calcined at the same temperature.

The surface acidity of the solids was evaluated by FT-IR spectroscopy, by adsorption of pyridine and subsequent desorption under heating at increasing temperatures. The bands due to adsorbed pyridine were intense after the adsorption process (before heating the solids) and also after heating at 100, 200 and, to a lower extent, at 300 °C, their intensities strongly decreasing after calcination at 400 °C and completely disappearing at 500 °C (Fig. 6). Integration of the area of the peaks allowed the acidity to be quantified (Table 5). Brönsted acidity strongly increased on pillaring, that is, it was much higher in the pillared solids than in natural Mt. The maximum values of Brönsted acidity corresponded to the solids calcined at 300 °C. However, Lewis acidity was also much higher for the pillared solids than for the natural Mt, and decreased progressively on heating.

Brönsted acidity appears in these solids mainly associated with the pillars and with the clay silanol groups. Brönsted acidity was clearly more pronounced for the pillared solids than for the parent Mt and, up to 200 °C, it was similar for the Ti-PILC and for the doped solids. However, at 300 and 400 °C, the doped solids showed a larger acidity than the undoped Ti-PILC, in particular at 300 °C, more than 120 μmol $g^{-1}$. That is, the presence of the dopants modified the strength of the acid centres. This evolution of acidity with temperature may be related to the BET specific surface area, also clearly higher for the doped solids, as discussed above. But it may also be related to the thermal behaviour of the polycations induced by the doping cations. In this sense, it was significant that Fe-, Cu- and Cr-doped Ti-PILC showed their highest acidity values after calcination at 200 °C.[34] All the solids showed no acidity at 500 °C, the sudden decrease of acidity of the Ag-doped solid when the calcination temperature was increased from 300 to 400 °C also being remarkable.

Lewis acidity in PILC is associated with exchangeable cations and $Al^{3+}$ cations with incomplete coordination. Intercalation removes exchangeable cations, and further calcination of the solids at 500 °C leads to the dehydroxylation of the polycations with an increase in the number of unsaturated $Al^{3+}$, increasing this acidity. The presence of the doping cations made acidity increase with respect to the solid treated with pure Ti solution, suggesting that these cations may also contribute to the acidity, which also suggests that these cations are adsorbed on the surface of the clay, being accessible to pyridine. This also agrees with the fact that the solids containing Ag, Nd or In showed lower acidity than the similar solids containing Fe, Cu and Cr,[34] the acidity being related to the amount of the doping cations fixed.

Because acidity is a surface property, it is appropriate to relate it to the specific surface area of the solids. The number of acid centres per square metre, values given in parentheses in Table 5, were higher for the doped solids than for the solid pillared with pure Ti. Thus, the increase in the amount of acid centres did not only depend on the larger accessible surface area of these solids, but on the true development of specific acid centres associated with the doping cations, which may be related to oxo bridges between the doping cations and Ti from the pillars, or between the doping cations and Si or Al from the clay.

The scanning electron micrographs of the pillared clays showed that the clay particles had a uniformly very rough surface, which was maintained in the doped solids (Fig. S2). However, although the solid pillared with Ti pillars had a more globular appearance, the doped solids were spongier, which agreed with the evolution of the specific surface area and the pore volume of the solids.

Band gap values of $TiO_2$ were estimated using the Tauc plot approximation.[52] This method allows determination of the band edge by using the following equation:[53]

$$\alpha h\nu = A\left(h\nu - E_g\right)^{1/2}$$

where $\alpha$, $h$, $\nu$, $E_g$ and $A$ stand for the adsorption coefficient, Planck constant, radiation frequency, band gap energy and a constant respectively.

From this equation, a plot of $(\alpha h\nu)^{1/2}$ *v.* $h\nu$, the so-called Tauc Plot,[53] shows a linear region just above the absorption edge whose extrapolation to the photon energy axis ($h\nu$) yields the semiconductor band gap value. The values calculated (Table S1) were in all cases lower than the band gap reported for anatase, decreasing with increase in the amount of dopant cation and when the solids were calcined, and decreasing as well when the

**Table 5. Brönsted (B) and Lewis (L) acidity (μmol g$^{-1}$) of natural montmorillonite and of the pillared solids after adsorption of pyridine and heating at different temperatures**

In parentheses, number of acid centres per surface area unit (μmol m$^{-2}$)

| | Room temperature | | 100 °C | | 200 °C | | 300 °C | | 400 °C | | 500 °C | |
|---|---|---|---|---|---|---|---|---|---|---|---|---|
| | B | L | B | L | B | L | B | L | B | L | B | L |
| Mt | 4.2 (0.053) | 22.7 (0.284) | 4.1 (0.051) | 20.8 (0.260) | 4.5 (0.056) | 12.1 (0.151) | 4.2 (0.053) | 11.8 (0.148) | 0 | 7.0 (0.088) | 0 | 0 |
| MtTi | 29.0 (0.177) | 32.5 (0.198) | 47.5 (0.290) | 27.5 (0.168) | 66.5 (0.405) | 19.5 (0.119) | 71.3 (0.435) | 16.8 (0.102) | 20.8 (0.127) | 15.2 (0.093) | 0 | 0 |
| MtTiAg10 | 22.3 (0.102) | 75.8 (0.346) | 38.9 (0.178) | 65.4 (0.299) | 70.7 (0.323) | 60.4 (0.276) | 134.5 (0.614) | 60.2 (0.275) | 33.9 (0.155) | 29.0 (0.132) | 0 | 0 |
| MtTiNd10 | 23.5 (0.111) | 76.9 (0.364) | 47.8 (0.227) | 75.0 (0.355) | 84.3 (0.400) | 71.5 (0.339) | 86.7 (0.411) | 63.2 (0.300) | 70.8 (0.336) | 58.0 (0.275) | 0 | 0 |
| MtTiIn10 | 33.1 (0.141) | 119.7 (0.509) | 58.0 (0.247) | 102.0 (0.434) | 79.8 (0.340) | 80.7 (0.343) | 128.2 (0.546) | 52.8 (0.225) | 71.3 (0.303) | 52.2 (0.222) | 0 | 0 |

**Table 6. Percentage elimination of methylene blue after 24 h**

| | First cycle | | Second cycle | |
|---|---|---|---|---|
| | With light | Without light | With light | Without light |
| Mt | 99.8 | 30.9 | 98.7 | 7.8 |
| MtTi | 99.8 | 31.8 | 98.7 | 0.0 |
| MtTiFe10 | 99.7 | 32.8 | 99.2 | 10.7 |
| MtTiCu10 | 99.8 | 58.2 | 99.6 | 2.0 |
| MtTiCr10 | 99.9 | 23.6 | 99.4 | 11.7 |
| MtTiAg10 | 99.8 | 39.3 | 98.8 | 0.0 |
| MtTiNd10 | 99.8 | 45.2 | 98.8 | 0.0 |
| MtTiIn10 | 99.8 | 32.8 | 99.3 | 3.5 |

other solids were compared with the MtTi-500 sample. So, both the amount and type of dopant cation, and the calcination temperature influenced the band gap, which reflects changes in the photocatalytic properties.

### *Removal of methylene blue*

The amount of methylene blue removed in adsorption experiments with sunlight or in the dark was evaluated using 5.0 mL of MB solutions and 50 mg of the adsorbents. The solids with higher amounts of doping elements, so those prepared from solutions containing 10 % of the dopants, were used. The MB elimination percentages after 24 h are summarised in Table 6.

It is remarkable that all the catalysts exhibited very high activities when the experiments were carried out under UV light. If fact, in the first cycle, MB was almost completely removed, reaching values between 99.7 and 99.9 %, and preventing any valid comparisons with the behaviour of these catalysts. The solids were tested in a second catalytic cycle, and although the activity decreased, this decrease was only ~1 %, so the values may be considered practically constant within experimental error.

The removal efficiency was noticeably lower when the experiments were carried out in the dark, circumstances that allowed comparison of the different solids. The parent Mt showed a rather high removal efficiency, close to 31 %, a value similar, and even higher, than those shown by some of the pillared solids. The solids doped with Ag, Nd, and particularly with Cu, showed enhanced removal efficiencies. The Cu sample had the highest BET specific surface area, but although this magnitude can influence the removal efficiency, it did not seem to be a determining factor, and the same can be said for the acidity, because solids with notable differences in these magnitudes showed very similar removal efficiencies. Quite surprising results were obtained when the materials were tested in a second cycle because solids that were very active in the first one strongly decreased in activity, which was zero in the second cycle for the Ag and Nd solids, and ~only 2 % in the case of the Cu solid. In contrast, other solids maintained a fair efficiency: the solids doped with Fe and Cr, and also the parent Mt. This behaviour seemed to be related to the interaction between the solids and MB, because the dye was strongly adsorbed on the solids (the solids were slightly blue even after careful washing for reuse), so removal was mainly due to adsorption, and to a much lesser extent to true degradation. So, the solids that more strongly bonded the dye in the first cycle must retain part of this dye after the recycling procedure, those positions being consequently blocked for the new adsorption cycle. In contrast, the dye weakly bonded to the other solids may be more successfully washed off during the recycling procedure. It may be considered

**Table 7. Kinetic study parameters obtained by fitting to mathematic models of pseudo-first order and pseudo-second order**

| | | Pseudo-first order | | | Pseudo-second order | | |
|---|---|---|---|---|---|---|---|
| Adsorbents | $q_e$ (mg g$^{-1}$) | $q_1$ (mg g$^{-1}$) | $k_1$ (min$^{-1}$) | $r^{2A}$ | $q_2$ (mg g$^{-1}$) | $k_2$ (g mg$^{-1}$ min$^{-1}$) | $r^{2A}$ |
| Mt | 7.39 | 5.44 | 1.57 | 0.54 | 7.87 | 0.01 | 0.992 |
| MtTiCr | 7.15 | 6.68 | 0.30 | 0.36 | 6.61 | 0.32 | 0.98 |
| MtTiFe | 7.47 | 6.82 | 0.33 | 0.51 | 7.19 | 0.24 | 0.998 |

[A]Statistical coefficient of determination.

that MB is positively charged and that adsorption is below the cation exchange capacity (CEC) of the clay, and largely below the adsorption values reported in the literature,[54] which suggests that cationic exchange should be the predominant adsorption mechanism. Results in Table 6 suggest that the dopant elements contribute to the degradation, and also to adsorption during the experiments in the dark. The possible leaching of these transition cations was not evaluated, but it should be considered that pillared clays incorporating transition cations have been used as catalysts in different oxidation reactions, and the leaching of the transition metals is usually very low, even negligible.[55]

Comparing the removal efficiency when the experiments were carried out under illumination or in the dark, it can be assumed that the amount of dye removed in the dark was due to adsorption, whereas the amount removed in the presence of light may be due to the sum of that removed by adsorption plus that removed by degradation, all the solids being effective catalysts for photodegradation of the dye, favoured by the easy access of dye molecules to the large surface area of the solids. The spectra of the solutions after finishing the process only showed the band corresponding to the residual presence of MB. However, new bands relating to intermediate degradation species were not recorded. This finding suggested the complete mineralisation of the dye, confirming the strong degradation efficiency of the catalysts.

## *Adsorption of trimethoprim*

### *Kinetic studies*

Natural Mt and the solids MtTiFe10 and MtTiCr10 were chosen for this study, because these are the solids that showed the best behaviour in MB adsorption. First, the time required for these solids to reach equilibrium in TMP adsorption experiments was determined. Removal percentages close to 75 % were obtained after only 5 or 10 min using the pillared solids as adsorbents, whereas 150 min was needed to reach the same adsorption percentage when using the original clay.

Degradation of TMP was evaluated on the natural Mt and on the pillared solids TiCr and TiFe in the dark. Degradation was observed after 15 min, although the resulting by-products could not be identified (the characteristic band from TMP decreased in intensity and shifted to a lower wavelength, Fig. S3). Both pillared clays maintained the same degradation effectiveness using natural sunlight, confirming their high activity. Pillared clays showed clear changes in the intensities and positions of the UV-vis bands, confirming the oxidation of TMP, whereas the parent Mt showed decolourisation, but not degradation, because no changes in the positions of the UV-vis bands were observed, but only a reduction of the intensities of the TMP bands. So, the removal was mainly due to adsorption, probably through hydrogen bonding between –$NH_2$ groups in TMP and Brönsted acidic sites in the solids.

Concerning the experiments carried out in the dark, pseudo-first-order and pseudo-second-order kinetic models were used to fit the experimental data, in order to examine the mechanism that controlled TMP adsorption onto these adsorbents.[56] The Largengren or pseudo-first-order equation obeys the following equation:[57]

$$q_t = q_e[1 - \exp(-k_1 t)] \quad (7)$$

where $k_1$ (mL min$^{-1}$) is a first-order constant, $q_t$ (mg g$^{-1}$) is the amount of TMP adsorbed at time $t$ (min), and $q_e$ (mg g$^{-1}$) is the amount of TMP adsorbed once the equilibrium has been reached. The pseudo-second-order model follows Eqn 8:[58]

$$q_t = \frac{k_2 q_e^2 t}{1 + k_2 q_e t} \quad (8)$$

where $k_2$ (g mg$^{-1}$ min$^{-1}$) is a second-order adsorption constant and the other variables have the same meaning as above.

The pseudo-second-order equation fitted the experimental data better (Table 7), confirming that the process was controlled by chemical adsorption. This suggested that there was a strong adsorbent–adsorbate interaction, and that there was more than one type of active site for the adsorption of the molecules. The constant showed a very low value for the natural Mt, increasing for the pillared clays, indicating that the intercalation of the polycations favoured the adsorption of TMP.

### *Equilibrium experiments*

To evaluate the efficiency of the adsorbents, equilibrium adsorption was studied as a function of the equilibrium concentration (Fig. 7). In all cases, the adsorption capacity of the adsorbents increased when increasing the initial TMP concentration. According to the Giles classification, the shapes of the isotherms corresponded to L2-type behaviour for Mt and MtTiFe10 and L4-type behaviour for MtTiCr10.[59] L-type or Langmuir isotherms have a convex, non-linear slope. In this case, the availability of the adsorption sites decreased when increasing the solution concentration. According to this classification, the L2-type curves indicated a saturation of the surface where the adsorbate has more affinity for the solvent than for the adsorbed molecules, whereas the adsorbents showing L4-type curves should have complete layers of adsorbed TMP, as confirmed by the fact that the isotherms reached a plateau.[60]

The regression coefficients for the Freundlich, Langmuir and Toth equations were always higher than 0.93 (Table 8). The best fitting was observed for the Langmuir model, suggesting that the adsorption occurred at identical and equivalent sites forming a monolayer, this being favourable in all cases because the equilibrium parameter $R_L$ is less than the unity.

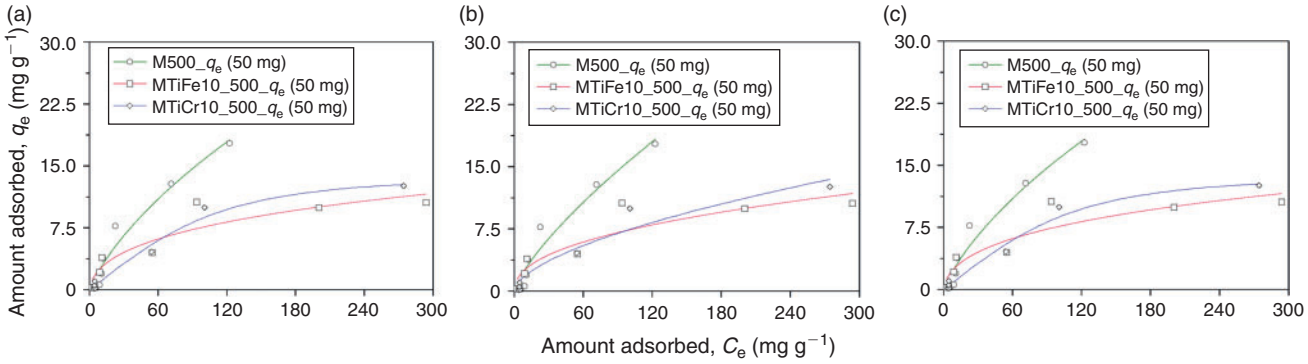


**Fig. 7.** Mathematical models of (a) Langmuir. (b) Freundlich and (c) Toth for adsorption of trimethoprim.

**Table 8. Parameters calculated for the equilibrium study of trimethoprim using the isotherms of Langmuir, Freundlich and Toth**

| | Langmuir | | | | Freundlich | | | Toth | | | |
|---|---|---|---|---|---|---|---|---|---|---|---|
| | $b$ (mL mg$^{-1}$) | $q_L$ (mg g$^{-1}$) | $r^{2A}$ | $R_L$ | $n$ | $k_F$ (mg$^{n+1}$ g$^{-1}$ mL$^{-1}$) | $r^{2A}$ | $q_T$ (mg g$^{-1}$) | $b$ (mL mg$^{-1}$) | $n$ | $R^2$ |
| MtTiCr | 0.008 ± 0.003 | 18.67 ± 3.11 | 0.98 | 0.96 | 1.70 ± 0.31 | 0.49 ± 0.28 | 0.97 | 13.80 ± 3.25 | 0.008 ± 0.002 | 2.20 ± 2.48 | 0.991 |
| MtTiFe | 0.022 ± 0.012 | 12.51 ± 1.91 | 0.95 | 0.90 | 2.33 ± 0.56 | 1.03 ± 0.54 | 0.93 | 256.95 ± 4137.8 | 0.128 ± 1.159 | 0.15 ± 0.64 | 0.935 |
| Mt | 0.009 ± 0.004 | 34.51 ± 10.61 | 0.98 | 0.92 | 1.34 ± 0.20 | 0.51 ± 0.26 | 0.97 | 1068.6 ± 30839 | 0.0006 ± 0.01 | 0.28 ± 1.69 | 0.974 |

[A]Statistical coefficient of determination.

## Conclusions

Mt was effectively pillared with Ti polycations incorporating small amounts of dopant cations. The final solids had large basal spacing, specific surface area, porosity and acidity. Powder X-ray diffraction patterns showed the typical reflections of expanded Mt. In the presence of light, the solids showed high photocatalytic activity for the removal of MB. Without light, the adsorption of TMP reached percentages of ~75 % after 5 or 10 min, compared with the 150 min needed for the natural clay to reach the same adsorption percentage. The pseudo-second-order kinetics model described the adsorption well, whereas the equilibrium Langmuir isotherm was the best for describing the adsorption mechanism.

## Supplementary material

Additional characterisation data for the solids are available from the Journal's website.

## Acknowledgements

The Spanish authors thank the Spanish Ministry of Economy and Competitiveness (MINECO) and the European Regional Development Fund (ERDF) (grant MAT2013–47811–C2–R) for financial support. The Brazilian group acknowledges support from Brazilian research funding agencies Fundação de Amparo à Pesquisa do Estado de São Paulo (FAPESP) (311767/2015–0 and 2016/01501–1), Coordenação de Aperfeiçoamento de Pessoal de Nível Superior (CAPES) and Conselho Nacional de Desenvolvimento Científico e Tecnológico (CNPq). Both groups thank the Spain–Brazil Interuniversity Cooperation Grant, funded by the Spanish Ministry of Education, Science and Sports (PHBP14/00003) and CAPES (317/15).

## References

[1] M. Qadir, D. Wichelns, L. Raschid-Sally, P. G. McCornick, P. Drechsel, A. Bahri, P. S. Minhas, The challenges of wastewater irrigation in developing countries. *Agric. Water Manage.* **2010**, *97*, 561. doi:10.1016/J.AGWAT.2008.11.004

[2] J. M. Guadayol, J. Caixach, J. Ribé, J. Cabanas, Extraction, separation and identification of volatile organic compounds from paprika oleoresin (Spanish type). *J. Agric. Food Chem.* **1997**, *45*, 1868. doi:10.1021/JF960266I

[3] H. Park, C. Vecitis, M. R. Hoffmann, Electrochemical water splitting coupled with organic compound oxidation: the role of active chlorine species. *J. Phys. Chem. C* **2009**, *113*, 7935. doi:10.1021/JP810331W

[4] M. E. Williams, J. A. Hestekin, C. N. Smothers, D. Bhattacharyya, Separation of organic pollutants by reverse osmosis and nanofiltration membranes: mathematical models and experimental verification. *Ind. Eng. Chem. Res.* **1999**, *38*, 3683. doi:10.1021/IE990140L

[5] L. Khenniche, F. Aissani, Preparation and characterization of carbons from coffee residue: adsorption of salicylic acid on the prepared carbons. *J. Chem. Eng. Data* **2010**, *55*, 728. doi:10.1021/JE900426A

[6] E. Fernandez, D. Hugi-Cleary, M. Lopez-Ramon, F. Stoeckli, Adsorption of phenol from dilute and concentrated aqueous solutions by activated carbons. *Langmuir* **2003**, *19*, 9719. doi:10.1021/LA030137D

[7] I. Efremenko, M. Sheintuch, Predicting solute adsorption on activated carbon: phenol. *Langmuir* **2006**, *22*, 3614. doi:10.1021/LA052100U

[8] S. R. Hughes, P. Kay, L. E. Brown, Global synthesis and critical evaluation of pharmaceutical data sets collected from river systems. *Environ. Sci. Technol.* **2013**, *47*, 661. doi:10.1021/ES3030148

[9] E. Marti, E. Variatza, J. L. Balcazar, The role of aquatic ecosystems as reservoirs of antibiotic resistance. *Trends Microbiol.* **2014**, *22*, 36. doi:10.1016/J.TIM.2013.11.001

[10] I. Oller, S. Malato, J. A. Sánchez−Pérez, Combination of advanced oxidation processes and biological treatments for wastewater decontamination − a review. *Sci. Total Environ.* **2011**, *409*, 4141. doi:10.1016/J.SCITOTENV.2010.08.061

[11] R. Hirsch, T. Ternes, K. Haberer, K. L. Kratz, Occurrence of antibiotics in the aquatic environment. *Sci. Total Environ.* **1999**, *225*, 109. doi:10.1016/S0048-9697(98)00337-4

[12] R. Lindberg, P.-A. Jarnheimer, B. Olsen, M. Johansson, M. Tysklind, Determination of antibiotic substances in hospital sewage water using solid phase extraction and liquid chromatography/mass spectrometry and group analogue internal standards. *Chemosphere* **2004**, *57*, 1479. doi:10.1016/J.CHEMOSPHERE.2004.09.015

[13] A. L. Batt, D. S. Aga, Simultaneous analysis of multiple classes of antibiotics by ion trap LC/MS/MS for assessing surface water and ground water contamination. *Anal. Chem.* **2005**, *77*, 2940. doi:10.1021/AC048512+

[14] D. W. Kolpin, E. T. Furlong, M. T. Meyer, E. M. Thurman, S. D. Zaugg, L. B. Barber, H. T. Buxton, Pharmaceuticals, hormones, and other organic wastewater contaminants in US streams, 1999–2000: a national reconnaissance. *Environ. Sci. Technol.* **2002**, *36*, 1202. doi:10.1021/ES011055J

[15] S. D. Costanzo, J. Murby, J. Bates, Ecosystem response to antibiotics entering the aquatic environment. *Mar. Pollut. Bull.* **2005**, *51*, 218. doi:10.1016/J.MARPOLBUL.2004.10.038

[16] S. H. Kim, H. K. Shon, H. H. Ngo, Adsorption characteristics of antibiotics trimethoprim on powdered and granular activated carbon. *J. Ind. Eng. Chem.* **2010**, *16*, 344. doi:10.1016/J.JIEC.2009.09.061

[17] H. Liu, J. Zhang, N. Bao, C. Cheng, L. Ren, C. Zhang, Textural properties and surface chemistry of lotus stalk-derived activated carbons prepared using different phosphorus oxyacids: adsorption of trimethoprim. *J. Hazard. Mater.* **2012**, *235–236*, 367. doi:10.1016/J.JHAZMAT.2012.08.015

[18] L. Nielsen, T. J. Bandosz, Analysis of sulfamethoxazole and trimethoprim adsorption on sewage sludge and fish waste derived adsorbents. *Microporous Mesoporous Mater.* **2016**, *220*, 58. doi:10.1016/J.MICROMESO.2015.08.025

[19] Z. Bekçi, Y. Seki, M. K. Yurdakoç, Equilibrium studies for trimethoprim adsorption on montmorillonite KSF. *J. Hazard. Mater.* **2006**, *133*, 233. doi:10.1016/J.JHAZMAT.2005.10.029

[20] C. I. Pearce, J. R. Lloyd, J. T. Guthrie, The removal of colour from textiles wastewater using whole bacterial cells: a review. *Dyes Pigments* **2003**, *58*, 179. doi:10.1016/S0143-7208(03)00064-0

[21] T. Robinson, G. McMullan, R. Marchant, P. Nigam, Remediation of dyes in textiles effluent: a critical review on current treatment technologies with a proposed alternative. *Bioresour. Technol.* **2001**, *77*, 247. doi:10.1016/S0960-8524(00)00080-8

[22] I. M. Banat, P. Nigam, D. Singh, R. Marchant, Microbial decolorization of textile-dye-containing effluents: a review. *Bioresour. Technol.* **1996**, *58*, 217. doi:10.1016/S0960-8524(96)00113-7

[23] V. S. Ferreira-Leitao, M. E. Andrade de Carvalho, E. P. S. Bon, Lignin peroxidase efficiency for methylene blue decolouration: comparison to reported methods. *Dyes Pigments* **2007**, *74*, 230. doi:10.1016/J.DYEPIG.2006.02.002

[24] K. Rida, S. Bouraoui, S. Hadnine, Adsorption of methylene blue from aqueous solution by kaolin and zeolite. *Appl. Clay Sci.* **2013**, *83–84*, 99. doi:10.1016/J.CLAY.2013.08.015

[25] D. Kavitha, C. Namasivayam, Experimental and kinetic studies on methylene blue adsorption by coir pith carbon. *Bioresour. Technol.* **2007**, *98*, 14. doi:10.1016/J.BIORTECH.2005.12.008

[26] S. Miao, Z. Liu, B. Han, J. Zhang, X. Yu, J. Du, Z. Sun, Synthesis and characterization of $TiO_2$–montmorillonite nanocomposites and their application for removal of methylene blue. *J. Mater. Chem.* **2006**, *16*, 579. doi:10.1039/B511426H

[27] A. Gil, M. A. Vicente, S. A. Korili, R. Trujillano, *Pillared Clays and Related Catalysts* **2010** (Springer: Heidelberg).

[28] M. A. Vicente, A. Gil, F. Bergaya, Pillared clays and clay minerals. In 'Handbook of Clay Science, 2nd Edition, Part A: Fundamentals'. (Eds F. Bergaya, G. Lagaly) **2013**, pp. 523–557 (Elsevier: Amsterdam).

[29] J. Schneider, M. Matsuoka, M. Takeuchi, J. Zhang, Y. Horiuchi, M. Anpo, D. W. Bahnemann, Understanding $TiO_2$ photocatalysis: mechanisms and materials. *Chem. Rev.* **2014**, *114*, 9919. doi:10.1021/CR5001892

[30] K. Nakata, A. Fujishima, $TiO_2$ photocatalysis: design and applications. *J. Photochem. Photobiol. Chem.* **2012**, *13*, 169. doi:10.1016/J.JPHOTOCHEMREV.2012.06.001

[31] L. V. Barbosa, L. Marçal, E. J. Nassar, P. S. Calefi, M. A. Vicente, R. Trujillano, V. Rives, A. Gil, S. Korili, K. J. Ciuffi, E. H. de Faria, Kaolinite–titanium oxide nanocomposites prepared via sol–gel as heterogeneous photocatalysts for dyes degradation. *Catal. Today* **2015**, *246*, 133. doi:10.1016/J.CATTOD.2014.09.019

[32] K. Kočí, V. Matejka, P. Kovár, Z. Lacny, L. Obalová, Comparison of the pure $TiO_2$ and kaolinite/$TiO_2$ composite as catalyst for $CO_2$ photocatalytic reduction. *Catal. Today* **2011**, *161*, 10. doi:10.1016/J.CATTOD.2010.08.026

[33] L. Chmielarz, P. Kuśtrowski, Z. Piwowarska, B. Dudek, B. Gil, M. Michalik, Montmorillonite, vermiculite and saponite based porous clay heterostructures modified with transition metals as catalysts for the DeNOx process. *Appl. Catal. B* **2009**, *88*, 331. doi:10.1016/J.APCATB.2008.11.001

[34] B. González-Rodríguez, R. Trujillano, V. Rives, M. A. Vicente, A. Gil, S. A. Korili, Structural, textural and acidic properties of Cu-, Fe- and Cr-doped Ti-pillared montmorillonites. *Appl. Clay Sci.* **2015**, *118*, 124. doi:10.1016/J.CLAY.2015.09.010

[35] J. T. Lin, S. J. Jong, S. Cheng, A new method for preparing microporous titanium pillared clays. *Microporous Mater.* **1993**, *1*, 287. doi:10.1016/0927-6513(93)80072-3

[36] H. Einaga, Hydrolysis of titanium(IV) in aqueous (Na,H)Cl solution. *J. Chem. Soc. Dalton Trans.* **1979**, 1917.

[37] S. Brunauer, P. H. E. Emmet, E. Teller, Adsorption of gases in multimolecular layers. *J. Am. Chem. Soc.* **1938**, *20*, 1553. doi:10.1021/JA01269A023

[38] B. C. Lippens, J. H. De Boer, Studies on pore systems in catalysis. *J. Catal.* **1965**, *4*, 319. doi:10.1016/0021-9517(65)90307-6

[39] F. Rouquerol, J. Rouquerol, K. Sing, *Adsorption by Powders and Porous Solids – Principles, Methodology and Applications* **1998** (Academic Press: London).

[40] T. Barzetti, E. Selli, D. Moscotti, L. Forni, Pyridine and ammonia as probes for FTIR analysis of solid acid catalysts. *J. Chem. Soc., Faraday Trans.* **1996**, *92*, 1401. doi:10.1039/FT9969201401

[41] F. J. del Rey-Pérez-Caballero, G. Poncelet, Microporous 18 Å Al-pillared vermiculites: preparation and characterization. *Microporous Mesoporous Mater.* **2000**, *37*, 313. doi:10.1016/S1387-1811(99)00274-7

[42] C. A. Emeis, Determination of integrated molar extinction coefficients for absorption bands of pyridine adsorbed on solid acid catalysts. *J. Catal.* **1993**, *141*, 347. doi:10.1006/JCAT.1993.1145

[43] I. Langmuir, The constitution and fundamental properties of solids and liquids. *J. Am. Chem. Soc.* **1916**, *38*, 2221. doi:10.1021/JA02268A002

[44] H. M. F. Freundlich, Over the adsorption in solution. *Z. Phys. Chem.* **1906**, *57*, 385.

[45] J. Toth, State equation of the solid–gas interface layers. *Acta Chim. Acad. Sci. Hung.* **1971**, *69*, 311.

[46] H. Guan, G. Guiochon, Properties of some C18 stationary phases for preparative liquid chromatography: II. Column efficacy. *J. Chromatogr. A* **1994**, *687*, 201. doi:10.1016/0021-9673(94)00774-8

[47] F. Gritti, G. Gotmar, B. J. Stanley, G. Guiochon, Determination of single component isotherms and affinity energy distribution by chromatography. *J. Chromatogr. A* **2003**, *988*, 185. doi:10.1016/S0021-9673(02)02084-8

[48] M. A. Vicente-Rodríguez, M. Suárez Barrios, M. A. Bañares Muñoz, J. D. López González, Comparative FT-IR study of the removal of octahedral cations and structural modifications during acid treatment of several silicates. *Spectrochim. Acta A* **1996**, *52*, 1685. doi:10.1016/S0584-8539(96)01771-0

[49] H. L. Del Castillo, A. Gil, P. Grange, Influence of the nature of titanium alkoxide and of the acid of hydrolysis in the preparation of titanium-pillared montmorillonites. *J. Phys. Chem. Solids* **1997**, *58*, 1053. doi:10.1016/S0022-3697(97)00006-1

[50] M. A. Vicente, M. A. Bañares-Muñoz, R. Toranzo, L. M. Gandía, A. Gil, Influence of the Ti precursor on the properties of Ti-pillared smectites. *Clay Miner.* **2001**, *36*, 125. doi:10.1180/000985501547295

[51] K. S. W. Sing, D. H. Everett, R. A. W. Haul, L. Moscou, R. A. Pierotti, J. Rouquerol, T. Siemieniewska, Reporting physisorption data for gas/solid systems with special reference to the determination of surface area and porosity. *Pure Appl. Chem.* **1985**, *57*, 603. doi:10.1351/PAC198557040603

[52] J. Tauc, Absorption edge and internal electric fields in amorphous semiconductors. *Mater. Res. Bull.* **1970**, *5*, 721. doi:10.1016/0025-5408(70)90112-1

[53] M. A. Butler, Photoelectrolysis and physical properties of the semiconducting electrode $WO_2$. *J. Appl. Phys.* **1977**, *48*, 1914. doi:10.1063/1.323948

[54] G. Rytwo, S. Nir, L. Margulies, Interactions of monovalent organic cations with montmorillonite: adsorption studies and model calculations. *Soil Sci. Soc. Am. J.* **1995**, *59*, 554. doi:10.2136/SSSAJ1995.03615995005900020041X

[55] L. A. Galeano, M. A. Vicente, A. Gil, Catalytic degradation of organic pollutants in aqueous streams by mixed Al/M-pillared clays (M = Fe, Cu, Mn). *Catal. Rev.* **2014**, *56*, 239. doi:10.1080/01614940.2014.904182

[56] Y. Xi, M. Mallavarapu, R. Naidu, Preparation, characterization of surfactants modified clay minerals and nitrate adsorption. *Appl. Clay Sci.* **2010**, *48*, 92. doi:10.1016/J.CLAY.2009.11.047

[57] S. Lagergren, About the theory of so-called adsorption of soluble substances. *K. Sven. Vetensk. Akad. Handl.* **1898**, *24*, 1.

[58] Y. S. Ho, G. McKay, Pseudo-second order model for sorption processes. *Process Biochem.* **1999**, *34*, 451. doi:10.1016/S0032-9592(98)00112-5

[59] C. H. Giles, D. Smith, A. Huitson, A general treatment and classification of the solute adsorption isotherm. I. Theoretical. *J. Colloid Interface Sci.* **1974**, *47*, 755. doi:10.1016/0021-9797(74)90252-5

[60] S. Z. Falone, E. M. Vieira, Adsorption/desorption of the explosive tetryl in peat and yellow−red argissol. *Quim. Nova* **2004**, *27*, 849. doi:10.1590/S0100-40422004000600002

Handling Editor: Kevin Wilkinson

*Environ. Chem.* **2017**, *14*, 267–278
doi:10.1071/EN16192_AC 

**Supplementary material**

# Doped Ti-pillared clays as effective adsorbents – Application to methylene blue and trimethoprim removal

*Beatriz González, Raquel Trujillano, Miguel A. Vicente, Vicente Rives, Emerson H. de Faria, Katia J. Ciuffi, Sophia A. Korili and Antonio Gil*

[A]Grupo de Investigación Reconocido Química del Estado Sólido, Materiales y Catálisis Heterogénea (GIR-QUESCAT), Departamento de Química Inorgánica, Universidad de Salamanca, 37008 Salamanca, Spain.

[B]Universidade de Franca, Avenida Dr Armando Salles Oliveira, Parque Universitário, 201, 14404-600, Franca/SP, Brazil.

[C]Departamento de Química Aplicada, Universidad Pública de Navarra, Campus de Arrosadía, E-31006-Pamplona, Spain.

[D]Corresponding author. Email: mavicente@usal.es

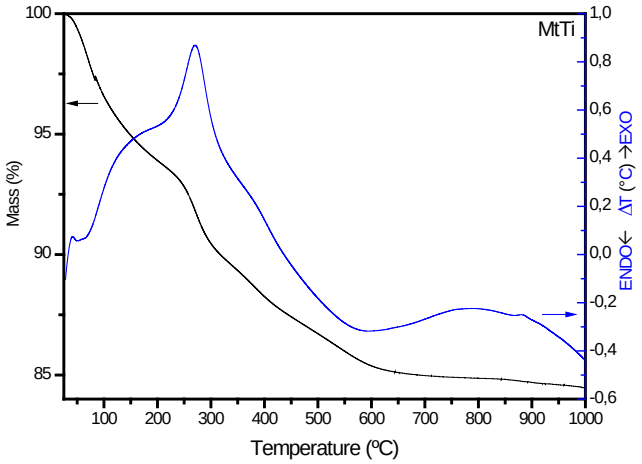


**Fig. S1.** Thermal curves (TG and DTA) of MtTi solid.

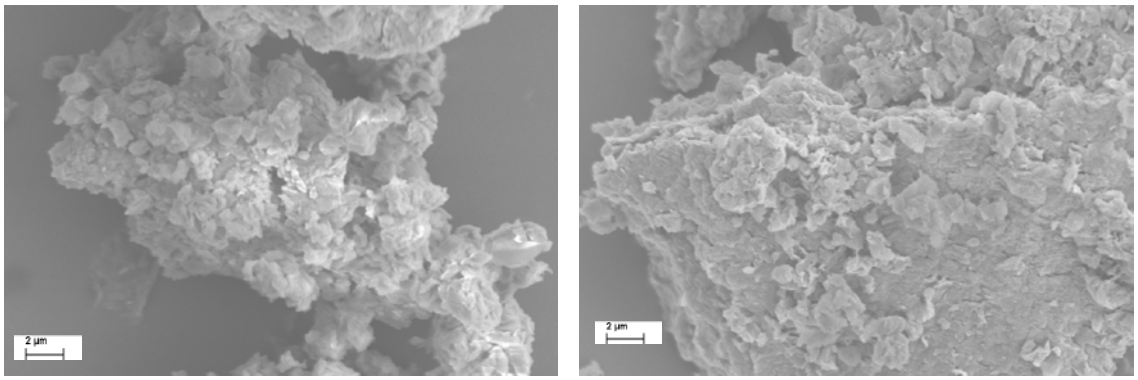


**Fig. S2**. SEM micrographs of MtTi (left) and MtTiIn10 (right).

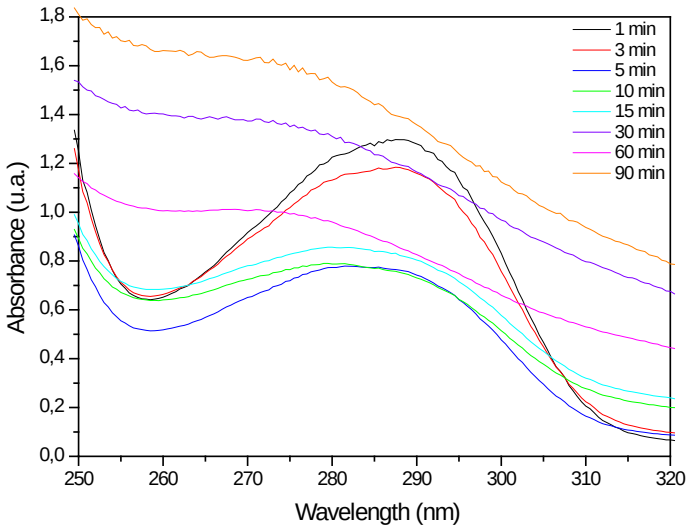


**Fig. S3.** UV spectra of MtTiCr solid.

**Table S1. Band gap values (eV) for intercalated and calcined samples**

| | Band gap energy (eV) | |
|---|---|---|
| | Intercalated | Pillared 500 °C |
| $TiO_2$ (rutile) | 3.05 | - |
| $TiO_2$ (anatase) | 3.20 | - |
| MtTi | - | 3.03 |
| MtTiCu5 | 3.16 | - |
| MtTiCu10 | 2.97 | 2.71 |
| MtTiCr5 | 2.99 | - |
| MtTiCr10 | 2.97 | 2.62 |
| MtTiIn5 | 3.16 | - |
| MtTiIn10 | 3.16 | 3.04 |